



NRC Publications Archive Archives des publications du CNRC

Effective interactions and adsorption of heterocyclic aromatic hydrocarbons in Kaolinite organic solutions studied by 3D-RISM-KH molecular theory of solvation

Hlushak, Stepan; Kovalenko, Andriy

This publication could be one of several versions: author's original, accepted manuscript or the publisher's version. / La version de cette publication peut être l'une des suivantes : la version prépublication de l'auteur, la version acceptée du manuscrit ou la version de l'éditeur.

For the publisher's version, please access the DOI link below. / Pour consulter la version de l'éditeur, utilisez le lien DOI ci-dessous.

Publisher's version / Version de l'éditeur:

<https://doi.org/10.1021/acs.jpcc.7b06414>

The Journal of Physical Chemistry C, 121, 40, pp. 22092-22104, 2017-09-15

NRC Publications Record / Notice d'Archives des publications de CNRC:

<https://nrc-publications.canada.ca/eng/view/object/?id=4edc6040-30b3-4f99-83b7-7138dee6142e>

<https://publications-cnrc.canada.ca/fra/voir/objet/?id=4edc6040-30b3-4f99-83b7-7138dee6142e>

Access and use of this website and the material on it are subject to the Terms and Conditions set forth at

<https://nrc-publications.canada.ca/eng/copyright>

READ THESE TERMS AND CONDITIONS CAREFULLY BEFORE USING THIS WEBSITE.

L'accès à ce site Web et l'utilisation de son contenu sont assujettis aux conditions présentées dans le site

<https://publications-cnrc.canada.ca/fra/droits>

LISEZ CES CONDITIONS ATTENTIVEMENT AVANT D'UTILISER CE SITE WEB.

Questions? Contact the NRC Publications Archive team at

PublicationsArchive-ArchivesPublications@nrc-cnrc.gc.ca. If you wish to email the authors directly, please see the first page of the publication for their contact information.

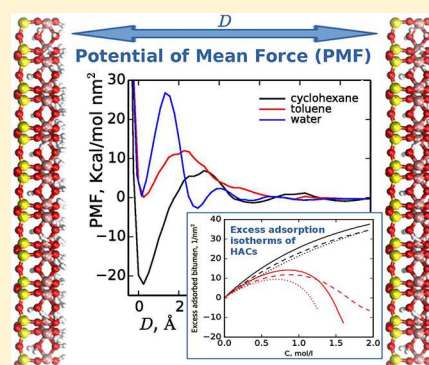
Vous avez des questions? Nous pouvons vous aider. Pour communiquer directement avec un auteur, consultez la première page de la revue dans laquelle son article a été publié afin de trouver ses coordonnées. Si vous n'arrivez pas à les repérer, communiquez avec nous à PublicationsArchive-ArchivesPublications@nrc-cnrc.gc.ca.



Effective Interactions and Adsorption of Heterocyclic Aromatic Hydrocarbons in Kaolinite Organic Solutions Studied by 3D-RISM-KH Molecular Theory of Solvation

Stepan Hlushak^{†,‡} and Andriy Kovalenko^{*,§,‡}[†]Department of Chemical and Materials Engineering, University of Alberta, Edmonton, Alberta T6G 2V4, Canada[‡]National Institute for Nanotechnology, Edmonton, Alberta T6G 2M9, Canada[§]Department of Mechanical Engineering, University of Alberta, Edmonton, Alberta T6G 2G8, Canada

ABSTRACT: We employ the molecular theory of solvation also known as the three-dimensional reference interaction site model with the Kovalenko–Hirata closure relation (3D-RISM-KH) to study adsorption of several heterocyclic aromatic hydrocarbons (acridine, benzothiophene, carbazole, dibenzothiophene, indole, and phenanthridine), which are intended to represent bitumen fragments on the surfaces of a single-sheet kaolinite nanoparticle in cyclohexane and toluene solvents. In addition to adsorption, we also examine solvent-mediated effective interactions between two kaolinite nanoparticles in organic and aqueous solutions. The proposed adsorption model serves as a simple prototype of suspensions formed during nonaqueous extraction of bitumen from oil sands of the Athabasca Basin. Using the proposed computational approach, excess adsorption isotherms of bitumen fragments on two different faces of kaolinite were calculated and compared in cyclohexane and toluene solvents at several temperatures. Almost all the studied



molecules show strong preference for adsorption on the octahedral aluminum hydroxide surface of kaolinite. While adsorption of the molecules on the tetrahedral silicon oxide surface is weaker, it is still significant compared to the octahedral surface and for some of the studied molecules adsorption appears to be stronger than for the octahedral surface. Due to the better surface and bulk solvation properties of toluene, the adsorption of the bitumen fragments in toluene is weaker than in cyclohexane. Potentials of mean force between kaolinite nanoplatelets in cyclohexane at several temperatures were calculated using the 3D-RISM-KH molecular theory of solvation. Evaluation of effective interactions by conventional molecular simulation techniques generally requires costly free energy integration and therefore is usually avoided by adopting simple and often unrealistic semiempirical effective potentials. On the other hand, the 3D-RISM-KH molecular theory of solvation offers a fully atomistic description with all-atom force fields and notable performance advantages over molecular simulations. Obtained in this way potentials of mean force in organic solvents exhibit complex oscillating behavior and generally possess deeper main minima and smaller aggregation barriers than the corresponding potentials in aqueous solution.

INTRODUCTION

The rise of petroleum usage across society is commonly associated with the invention of the internal combustion engine and with the subsequent growth of the automotive and aviation industries and the tremendous importance of petroleum to the chemical industry. It is used in synthesis of solvents, fertilizers, adhesives, and plastics. With the gradual depletion of conventional petroleum reserves, production is switching to unconventional ones such as oil sands and oil shales. Oil sands, also known as tar sands or more technically bituminous sands, are a type of unconventional petroleum deposit found in large quantities in Canada, Venezuela, Kazakhstan, and Russia.¹ Oil sands have only recently been considered to be part of the world's unconventional oil reserves, as new technologies stimulated by high oil prices allowed profitable extraction and processing of bitumen. The total oil sand reserves are estimated to constitute about 30% of world oil deposits.² Athabasca oil sands is the only suitable deposit for surface mining. It is one of

the largest natural bitumen deposits in the world containing about 1.7 trillion barrels of bitumen, about 10% of which is estimated to be economically recoverable.³ This fact makes the total proven reserves of Canada the third largest in the world, after conventional oil in Saudi Arabia and the Orinoco oil sands in Venezuela.^{4,5}

Technically, oil sands can be described as a mixture of sand, water, clay, and hydrocarbon-rich bitumen. Current mining operations use the Clark hot water extraction process,⁶ which was also the first process used commercially⁷ to separate bitumen from other components. One of the main drawbacks of the current hot water extraction process is excessive use of water, which could affect the aquatic ecosystem of the Athabasca River. About 4 times more water is generally

Received: June 29, 2017

Revised: September 13, 2017

Published: September 15, 2017

required to produce a unit of bitumen using aqueous extraction processes, and almost all that water ends in tailing ponds. The occupation of significant areas of land by large volumes of wet tailings is one of the most severe problems of the oil sands industry.

Introduction of nonaqueous extraction processes is anticipated to significantly decrease CO₂ emissions and the use of water, and therefore to eliminate most of the environmental implications of mining. While the initial research on this technology started a few decades ago, no nonaqueous extraction has been implemented commercially to date, which is explained by the significant technical challenges of engineering environmentally safe and energy efficient processes. The main difficulties are related to the properties of organic solvents which are quite expensive, commonly toxic and flammable and, therefore, cannot be released to the environment. Unfortunately, the currently proposed nonaqueous extraction processes suffer from insufficient solvent recovery from the waste (also termed as “gangue”). Complete recovery often requires several additional steps such as distillation and drying, which are energetically expensive.

Selection of an optimal solvent for nonaqueous extraction is a challenging problem, as the hypothetical ideal solvent should be affordable, nontoxic (green), and easily recoverable, and should provide good bitumen desorption. To date, a number of different solvents and solvent mixtures have been tested for bitumen extraction.^{8–12} Nikakhtari et al.⁸ screened 13 different solvents and mixtures for bitumen desorption, solvent recovery, and residual fines in extracted bitumen, and found that cyclohexane and isoprene are the most promising among the studied solvents for commercial utilization. Both cyclohexane and toluene showed excellent bitumen recovery (94.4 and 96.3%).⁸ However, only cyclohexane was found to be the most suitable solvent for the nonaqueous extraction of the Alberta oil sands based on the selection criteria which additionally included important technological and environmental factors such as removal rate from the extraction tailings, low residual solvent concentration in the tailings after drying, and low content of fine solids in the extracted bitumen.⁸ Bitumen recovery also seems to critically affect the solvent recovery, as the lower level of residual bitumen in the gangue generally leads to a better solvent recovery.¹³ This fact suggests that the desorption of bitumen is one of the most important features that should be maximized during the process design and optimization.

To date, adsorption of the organic molecules on clay surfaces has mainly been studied by the density functional,^{14–19} molecular dynamics,^{20–22} and 3D-RISM (three-dimensional reference interaction site model)^{19,23–25} approaches. Most of these studies observed preferential adsorption of organic molecules on the hydrophilic aluminum hydroxide surface of kaolinite. Among the recent studies of organic adsorption on kaolinite, we would like to highlight the molecular dynamics study of Underwood et al.,²⁰ who observed predominant adsorption of decane and decanoic acid from aqueous solution on the siloxane surface of kaolinite and complete withdrawal of the molecules from the hydroxyl surface. Remarkably, the decane molecules are adsorbed parallel to the surface and form stacks upon each other. Such a multilayered adsorption pattern is also observed for decanoic acid. However, in the latter case, the presence of the polar hydrophilic COOH group makes the adsorption of the acid on the siloxane surface less preferable compared to purely hydrophobic decane molecules. Preferred

adsorption of methylene blue on the hydrophobic siloxane surface of kaolinite was also observed by Greathouse et al.²² Three different preferential orientations of methylene blue molecule on the siloxane surface, two of which were perpendicular and one was parallel to the surface, were identified by the authors. The structure and energetics of the adsorbed methylene blue were mostly governed by strong interfacial rather than solvation forces.

Adsorption of the bitumen fragments on the kaolinite surfaces in organic solvents was also examined experimentally and theoretically by Fafard et al.²⁴ and Huang et al.²⁵ Because of the insufficiently developed methodology, it was still not possible to directly compare the experimental and theoretical adsorption isotherms. However, the application of the 3D-RISM molecular theory of solvation allowed us to obtain important molecular insights on the chemical mechanisms of the preferential adsorption of bitumen fragments on the surfaces of kaolinite. The main prediction of these studies was that the aluminum hydroxide surface of kaolinite is preferred for acridine and phenanthridine adsorption due to a strong hydrogen bonding with the pyridinic N atoms. The adsorption of the other studied heterocyclic aromatic hydrocarbons (HACs) was much weaker. In refs 24 and 25, the theoretical analysis of the adsorption modeling by the molecular theory of solvation was mainly focused on the determination of optimal adsorbate configurations and their redistribution near kaolinite surfaces. Additionally, the amount of adsorbate near kaolinite surfaces was quantified from the information provided by the spatial distribution functions of the 3D-RISM-KH theory (3D-RISM model with the Kovalenko–Hirata closure relation). However, the adsorption isotherms were not calculated from the spatial distributions provided. In the current study we will try to more thoroughly examine the adsorption picture HACs predicted by the molecular theory of solvation by estimating and examining the excess amount of adsorbed molecules per unit of surface area of different kaolinite surfaces. We will also try to compare the predicted adsorption picture in the aromatic toluene and aliphatic cyclohexane hydrocarbon solvents.

Despite the exemplary performance demonstrated by cyclohexane for bitumen extraction, the content of fines in recovered bitumen was 1.4%,⁸ which is roughly 3 times larger than the maximum allowed for pipeline transport. In order to remove the fines, special costly procedures are required, such as destabilization by polymeric additives, which leads us to an interesting problem of stability of clay suspensions.

Aqueous suspensions of colloidal clays are known to exhibit a diversity of complex phase behaviors, which include phase separation between colloid-rich and colloid-poor phases, sol–gel transitions, emergence of glass and equilibrium gel phases, and hypothesized empty liquid states.^{26–29} This richness of phenomena motivated active experimental and theoretical research. Theoretical efforts to understand the emergence of gel phases in colloidal clay suspensions resulted in a number of simulation studies that advocated coarse-grained colloidal clay models for an explanation of these important phenomena.

Using a simple model of infinitely thin disks with embedded quadrupole moments, Dijkstra, Hansen, and Madded^{30,31} identified the so-called “house of cards” nanoparticle configuration, which was first proposed by Hofmann³² and Van Olphen.³³ Together with a few additional arrangements, this configuration of clay particles was observed in more refined models of clay.^{34–36} Another important insight obtained from

coarse-grained clay models is the so-called “overlapping coins” configuration. This arrangement was recently predicted by a realistic model of clay nanoparticles composed of multiple pseudosites interacting by the Lennard-Jones (LJ) and screened Coulomb potentials.^{34–36} The new model appeared to be accurate up to the salt screening length scale and provided a more realistic picture of the interactions between particles at short separations. The effect of clay charge anisotropy on gelation and glass formation³⁶ was investigated.^{35,36} By varying the charge of the pseudosites, and depending on the charge anisotropy, either liquid–gel or liquid–glass transitions were favored. The probability of different particle configurations was found to be highly dependent on the screening of the electrostatic interactions, i.e., on the salt concentration, and also on the concentration of clay. In the latter case, one could observe either phase separation between a weakly percolated gel and a fluid of stacked clusters, or a gel formation of large clusters of stacks by varying the concentration of the clay.³⁷ Additionally, at high salt concentrations (high screening), a percolation network configuration of face-to-face stacked platelets is formed.

While these simple simulation models of clays provided valuable insights on the structure and phase behavior of clay suspensions, their predictive capabilities are limited due to an oversimplified description of the electric double layers (at the level of Debye–Hückel theory), and a complete neglect of solvation of mineral surfaces and solvent structural effects. In order to take into account these important solvation effects, it is necessary to employ fully molecular models of both mineral surfaces and solvent. In our previous study,²³ we have proposed the 3D-RISM-KH molecular theory of solvation to estimate effective interactions between different surfaces of kaolinite nanoparticles in the form of the potential of mean force (PMF) and to analyze the adsorption structure of aqueous electrolyte species on mineral surfaces of kaolinite. The calculated PMFs between kaolinite nanoparticles exhibited nontrivial solvent structural effects such as oscillations at short ranges and solvation related differences in interactions between different surfaces of kaolinite. More importantly, a solvent-separated state of interacting nanoparticles was identified. This state is characterized by a stable second PMF minimum with energy close to zero, and corresponds to an arrangement when the two interacting faces are separated by a single “stabilizing” layer of solvent. Surprisingly, but from the free energy standpoint, the solvent-separated state appeared to be more probable than the state of direct contact in the cases when the interacting surfaces were similar.²³

Despite the significant research progress in the area of aqueous clay suspensions, the scientific literature on the suspensions of clays in organic solvents is less abundant. This fact, however, does not reflect the true industrial and technological importance of these systems. A perfect example of the technological importance of nonaqueous clay suspensions and also a motivation of current study is the problem of removal of fines from diluted bitumen during the process of nonaqueous extraction of bitumen from oil sands of the Athabasca Basin. Accurate determination of the effective interactions between the nanoparticles in colloidal suspensions is crucial for the understanding of their rich phase behavior. Evaluation of the interactions by conventional molecular simulation techniques requires application of costly free energy integration techniques and, therefore, is avoided by adopting simple and often unrealistic semiempirical effective potentials.

In order to obtain effective interactions in nonaqueous clay suspensions and to study the adsorption of several heterocyclic aromatic compounds from organic solvents on kaolinite surfaces, we employ the three-dimensional reference interaction site model with the Kovalenko–Hirata closure relation, also known as the 3D-RISM-KH molecular theory of solvation.^{38–41}

The 3D-RISM-KH molecular theory of solvation is a statistical mechanical method based on the integral equation theory of liquids, which predicts solvation effects in realistic complex systems and reproduces various structural and phase transitions in complex associating liquids and mixtures^{42,43} with full accounting for the interplay of both electrostatic and nonpolar effects, such as hydrogen bonding and solvophobic forces.⁴⁰ The 3D-RISM-KH theory was successfully applied to study hydration structure, potentials of mean force of ion pairs, ionic ordering and clustering in electrolyte solutions in a wide range of concentrations,^{38–40,44} aggregation of petroleum asphaltene in water-saturated chloroform solvent,⁴⁵ self-assembly and conformations of synthetic organic supra-molecular rosette nanotubular architectures,⁴⁶ gelation of oligomeric polyelectrolytes in different solvents,⁴⁷ molecule–surface recognition,²⁵ association of biomolecules in solution,⁴⁸ effective interactions of cellulose microfibrils in hemicellulose hydrogel,⁴⁹ and kaolinite nanoparticles in colloidal clay suspensions.²³

■ BRIEF OVERVIEW OF THE 3D-RISM-KH MOLECULAR THEORY OF SOLVATION

The 3D-RISM integral equation theory is used to determine the 3D distribution functions of solvent interaction sites around the solute molecule.^{41,50–59} The corresponding 3D-RISM integral equation

$$h_{\gamma}^{uv}(\mathbf{r}) = \sum_{\alpha} \int d\mathbf{r}' c_{\alpha}^{uv}(\mathbf{r} - \mathbf{r}') \chi_{\alpha\gamma}^{vv}(r') \quad (1)$$

is solved for the 3D total and direct correlation functions $h_{\gamma}^{uv}(\mathbf{r})$ and $c_{\gamma}^{uv}(\mathbf{r})$ of solvent site γ around the solute molecule, where the radially dependent site–site susceptibility of pure solvent $\chi_{\alpha\gamma}^{vv}(r)$ is an input to the 3D-RISM theory.

While being sufficiently rigorous, the 3D-RISM equation is incomplete and cannot be solved without additional assumptions. Therefore, the 3D-RISM equation has to be complemented with a closure relation between the total and direct correlation functions which involves the interaction potential between interaction sites of solution species specified with a molecular force field. Because the exact closure has a nonlocal functional form expressed as an infinite diagrammatic series in terms of multiple integrals of the total correlation function⁶⁰ (which appear to be poorly convergent), direct calculations of the exact closure are computationally intractable. Special approximations with analytical features that properly represent physical characteristics of the system, such as long-range asymptotics and short-range features of the correlation functions related to the solvation structure and thermodynamics, are used instead. In the current work, the 3D-RISM integral equation (eq 1) is complemented with the Kovalenko and Hirata (KH) closure approximation,^{41,54,56,57,59} which is a combination of the so-called hypernetted chain (HNC) and the mean spherical approximation (MSA)⁶⁰ closures. The KH closure reads

$$g_{\gamma}^{uv}(\mathbf{r}) = \begin{cases} \exp(-\beta u_{\gamma}^{uv}(\mathbf{r}) + h_{\gamma}^{uv}(\mathbf{r})) & \text{for } g_{\gamma}^{uv}(\mathbf{r}) \leq 1 \\ -c_{\gamma}^{uv}(\mathbf{r}) & \\ 1 - \beta u_{\gamma}^{uv}(\mathbf{r}) + h_{\gamma}^{uv}(\mathbf{r}) & \text{for } g_{\gamma}^{uv}(\mathbf{r}) > 1 \\ -c_{\gamma}^{uv}(\mathbf{r}) & \end{cases} \quad (2)$$

where $g_{\gamma}^{uv}(\mathbf{r}) = h_{\gamma}^{uv}(\mathbf{r}) + 1$ is the 3D density distribution function and $u_{\gamma}^{uv}(\mathbf{r})$ is the 3D interaction potential between site γ of solvent “v” and the whole solute molecule “u”. The interaction term, $-\beta u_{\gamma}^{uv}(\mathbf{r})$, between solute “u” and solvent site γ is specified by a molecular force field and scaled by the inverse thermodynamic temperature $\beta = (k_{\text{B}}T)^{-1}$. The KH approximation applies the HNC closure to the regions of density profile depletion, $g(r) < 0$, and the MSA closure to the regions of density enrichment, $g(r) > 0$. This combined scheme shows success in describing important features of the distribution functions such as long-range enhancement tails for the critical regime and high peaks for association effects in molecular fluids in a wide density range from gas to liquid. Moreover, applications of the HNC counterpart at density depletion regions eliminates the important drawback of the MSA theory, that produces unphysical negative values of the distribution functions at high densities and strong association, or for strongly repulsive potentials.^{61–64} On the other hand, due to the MSA linearization, the KH closure underestimates the height of strong associative peaks of the 3D site distribution functions because of the MSA linearization applied to them.^{54,65} Luckily, it somewhat widens the peaks and, therefore, quite accurately reproduces the coordination numbers of the solvation structure.

The site–site susceptibility function of pure solvent consists of the intra- and intermolecular parts:

$$\chi_{\alpha\gamma}^{vv}(r) = \omega_{\alpha\gamma}^{vv}(r) + \rho_{\alpha}^v h_{\alpha\gamma}^{vv}(r) \quad (3)$$

where $h_{\alpha\gamma}^{vv}(r)$ is the site–site total correlation function, and $\omega_{\alpha\gamma}^{vv}(r)$ is the intramolecular correlation function normalized as $4\pi \int_0^{\infty} r^2 dr \omega_{\alpha\gamma}^{vv}(r) = 1$ which represents the geometry of solvent molecules. For rigid species with site separations $l_{\alpha\gamma}$, it is expressed in the direct space in terms of δ -functions as $\omega_{\alpha\gamma}(r) = \omega_{\alpha\gamma}(r - l_{\alpha\gamma}) / (4\pi l_{\alpha\gamma}^2)$ and for numerical calculations is specified in the reciprocal space as $\omega_{\alpha\gamma}(k) = j_0(kl_{\alpha\gamma})$, where $j_0(x)$ is the zero-order spherical Bessel function. (It is implied that $\omega_{\alpha\gamma}^{vv}(r) = 0$ for sites α and γ on different species, and $l_{\alpha\alpha}^{vv} = 0$.)

The potential of mean force (PMF) between kaolinite nanoparticles is calculated as a sum of the Lennard-Jones dispersive energy contribution, $U_{\text{LJ}}(D)$, the electrostatic interaction energy contribution, $U_{\text{C}}(D)$, and the solvation energy contribution, $\mu_{\text{sol}}^{\text{KH}}(D) - \mu_{\text{sol}}^{\text{KH}}(D_{\text{max}})$:

$$\text{PMF}(D) = U_{\text{LJ}}(D) + U_{\text{C}}(D) + \mu_{\text{sol}}^{\text{KH}}(D) - \mu_{\text{sol}}^{\text{KH}}(D_{\text{max}}) \quad (4)$$

where D denotes separation between the surfaces of the platelets, $\mu_{\text{sol}}^{\text{KH}}(D)$ denotes the solvation free energy, and D_{max} is the maximal separation at which the solvation free energy is normalized to be zero.

The solvation free energy of solute nanoparticles in multicomponent solution described by the 3D-RISM-KH molecular theory of solvation can be presented in a closed analytical form:

$$\mu_{\text{sol}}^{\text{KH}} = k_{\text{B}}T \sum_{\gamma} \rho_{\gamma} \int d\mathbf{r} \left[\frac{1}{2} h_{\gamma}^2(\mathbf{r}) \Theta(-h_{\gamma}(\mathbf{r})) - c_{\gamma}(\mathbf{r}) - \frac{1}{2} h_{\gamma}(\mathbf{r}) c_{\gamma}(\mathbf{r}) \right] \quad (5)$$

where $\Theta(r)$ denotes the Heaviside step function.

MODELS OF BITUMEN FRAGMENTS, SOLVENTS, AND NANOPARTICLES

In order to assess the chemical interactions of bitumen macromolecules with kaolinite nanoparticles in cyclohexane and toluene, we represent the former as sufficiently small heterocyclic aromatic compounds (HACs) denoted as bitumen fragments. The following bitumen fragments were studied in this work: acridine, benzothiophene, carbazole, dibenzothiophene, indole, and phenanthridine. They are depicted in Figure 1, structures a, b, c, d, e, and f, respectively. Cyclohexane and

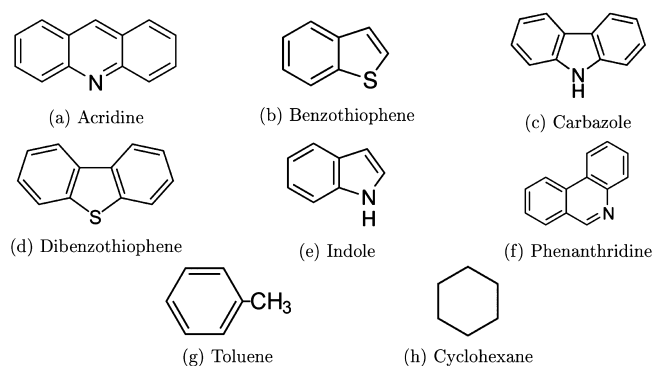


Figure 1. Heterocyclic aromatic carbon (HAC) molecules with toluene and cyclohexane solvents included in this study.

toluene solvents are depicted in Figure 1, structures g and h, respectively. The molecules are described as rigid bodies using the nonbonded parameters of the OPLS-aa force field and partial charges derived from geometry minimization in a vacuum with the PM7 method of the MOPAC quantum chemistry package.⁶⁶ Cyclohexane and toluene solvents are described using the OPLS-aa force field. The equilibrium conformations of bitumen fragments and solvents were obtained by minimizing positions of atoms in a vacuum using the PM7 method of the MOPAC package.⁶⁶

Calculations using the 3D-RISM-KH molecular theory of solvation require as an input the mass density and the dielectric properties of the solvent. The latter are assumed to be constant and independent of the concentration of the fragments in solution, and the value was set to 2.023. In order to study the temperature dependence of the adsorption of bitumen fragments on kaolinite, we performed calculations at three different temperatures: 298.15, 273.15, and 323.15 K. The concentration dependence of the mass density of the cyclohexane-fragment solution at different temperatures was obtained by fitting the results of separate molecular dynamics simulations at constant external pressure conditions. The simulations were performed with the LAMMPS package.⁶⁷

The molecular model of a single-layer kaolinite platelet was built similarly as in our previous work,²³ by populating a unit cell of kaolinite in two dimensions and cleaving a plate out of the resulting plane. The positions of the H atoms of the hydroxyl groups for every mutual orientation were optimized

by minimizing the energy of the platelet in a vacuum using the CLAYFF force field⁶⁸ as implemented in the LAMMPS molecular dynamics simulation package.⁶⁷ Nanoplatelets constructed with the outlined methodology possess a permanent dipole moment of about 39 e·Å oriented perpendicular to the platelet surface. This construction is in agreement with the experimental observations of Gupta and Miller,⁶⁹ who established that the tetrahedral siloxane surface of kaolinite is negatively charged, while the octahedral aluminum hydroxide surface becomes negatively charged at neutral pH conditions. Thus, the electrostatic interactions between the platelets seem to favor the contact of positively charged hydrophilic aluminum hydroxide surface with negatively charged hydrophobic siloxane surface, and disfavor the two other platelet arrangements.

Two types of 3D-RISM-KH calculations were performed. The first type was aimed at determining the PMF between two kaolinite nanoparticles, and involved multiple subcalculations at different distances between nanoparticles. The calculations were performed in $100 \times 100 \times 90$ Å unit cells, each of which contained two kaolinite nanoparticles at different distances. The cells were discretized into a grid of $260 \times 260 \times 500$ points. The PMF was assembled from the results of approximately 50 different calculations at 50 different distances between the platelets for each solvent system studied. The second type of calculations aimed at determining the excess adsorption isotherms of bitumen fragments on kaolinite surfaces. In this case, the calculations were performed in a $120 \times 120 \times 85$ Å unit cell for around 100 different solvent compositions, each with a different concentration of the corresponding bitumen fragment. The cell was discretized into a grid of $240 \times 240 \times 170$ points. In order to calculate the excess adsorption isotherm, the unit cell was divided into two parts, each containing a different kaolinite face. Then the excess number of solvent molecules of each type was calculated in each of the two cell parts in a cylinder region perpendicular to the nanoplate and passing through the center of the nanoplate (see Figure 2). The

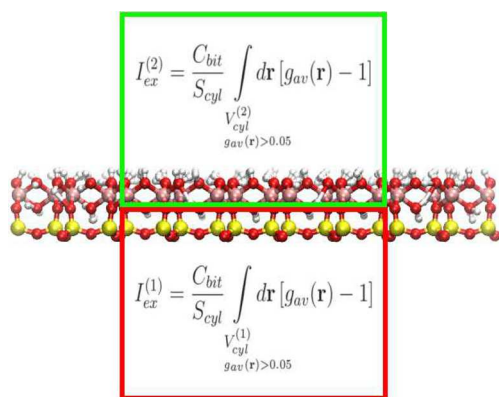


Figure 2. Schematic representation of the approach for calculation of excess adsorption.

radius of the cylinder region was selected to be 2 times smaller than the radius of the nanoplate in order to avoid calculation of excess adsorption on the edges of the nanoplates. Thus, the excess number of adsorbed bitumen fragments per surface area is calculated according to the following formula:

$$I_{ex}^{(f)} = \frac{C_{bit}}{S_{cyl}} \int_{V_{cyl}^{(f)}}_{g_{av}(\mathbf{r}) > 0.05} d\mathbf{r} [g_{av}(\mathbf{r}) - 1] \quad (6)$$

where C_{bit} is the concentration of bitumen fragments (number of molecules per volume unit), S_{cyl} is the cross-section surface area of the cylinder, $g_{av}(\mathbf{r})$ is the site-averaged solute–solvent spatial distribution function, and $V_{cyl}^{(f)}$ denotes the volume of the cylinder part corresponding to the face f of the nanoparticle. In order to avoid a negative contribution from the volume occupied by the nanoparticle, the integration in expression 6 is performed only in the areas where the spatial distribution function $g_{av}(\mathbf{r})$ is larger than a small value (0.05 in the present case).

Similarly to the scheme of the calculations of the excess adsorption isotherms outlined in Figure 2, the laterally averaged distribution functions presented in Figure 3 were obtained by averaging across the cross section of the cylinder region, which is perpendicular to the nanoplate and passes through the center of the latter.

RESULTS AND DISCUSSION

Solvation of Kaolinite Surfaces. The details of the surface specific solvation of kaolinite by cyclohexane and toluene solvents are presented in Figure 4, parts a and b, respectively. The presented 3D distribution functions possess highly localized density enhancements which are located near the centers of Si–O hexagonal rings on the silicon oxide surface and centers of the Al–O rings on the aluminum hydroxide surface. In the latter case the isosurface density patterns are more irregular due to a “randomized” orientation of the surface hydroxyl groups. It should be noted that the aluminum hydroxide surface is rigid in the RISM-3D-KH approach; i.e., the surface hydroxyl groups are not flexible during the modeling. Thus, the effects of the hydrogen bonding between the surface and the molecules might not be fully taken into account. This defect, however, should be partly alleviated by the precise averaging over the solvent degrees of freedom provided by the RISM-3D-KH theory of solvation. Therefore, the adopted approach should yield at least a representative picture of the aluminum hydroxide surface solvation.

Among the two studied solvents, toluene seems to possess better surface solvation properties compared to cyclohexane, as the corresponding density isosurfaces around kaolinite nanoparticles occupy more area and are more abundant. The distribution function isovalues plotted in Figure 4 are also higher for toluene (2.5) than for cyclohexane (1.65) solvent. Thus, the kaolinite surfaces seem to be better solvated in toluene than in cyclohexane, which will have important implications on the potential of mean force between the interacting kaolinite surfaces and on the adsorption of small molecules in these solvents.

Among the two surfaces of kaolinite, the aluminum hydroxide surface seems to be better solvated in both toluene and cyclohexane than the silicon oxide surface. This fact could be observed in Figure 4, where the density enhancements near the aluminum hydroxide surface are larger than near the silica oxide surface for both solvents. It is interesting to note that the methyl group of toluene shows some preference for the silicon oxide surface of kaolinite. The corresponding density enhancements are located near the centers of the hexagonal Si–O rings on the surface and could be clearly observed at the bottom of Figure 4b. This fact might indicate that the silicon oxide surface

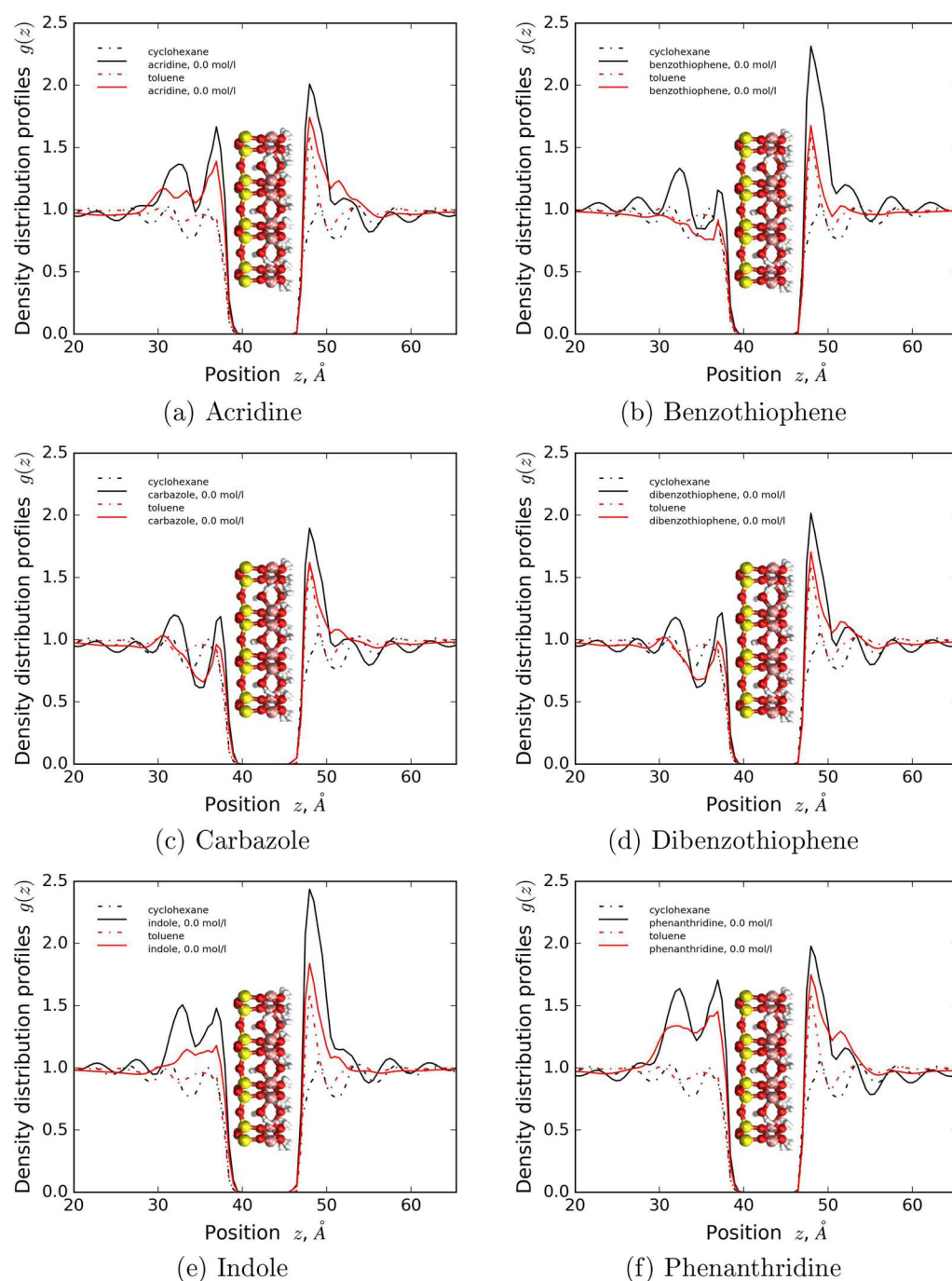


Figure 3. Laterally averaged distribution function profiles across the simulation box of cyclohexane, toluene, and HAC bitumen fragments in these two solvents, perpendicular to the surfaces of kaolinite platelet at 293.15 K and zero concentrations of the HACs. The planes containing oxygen atoms of silicon oxide and aluminum hydroxide surfaces of the nanoparticle are located at 40.0 and 44.35 Å, respectively.

is better solvated in toluene than in cyclohexane solvent. However, the examination of the laterally averaged density distribution functions near the silica oxide surface in **Figure 3** reveals that the corresponding profiles of toluene and cyclohexane are quite similar. The latter exhibits a larger oscillation amplitude and possesses a slightly larger first density peak.

Adsorption Structure and Isotherms. While the adsorption of several bitumen fragments on kaolinite in toluene and heptane has already been studied experimentally and theoretically,^{24,25} the adsorption behavior of bitumen fragments in cyclohexane has not been examined yet. As we have

mentioned, the theoretical analysis of the adsorption modeling by the molecular theory of solvation in the previous studies was mainly focused on the determination of optimal adsorbate configurations and their redistribution near kaolinite surfaces. The amount of adsorbate near kaolinite surfaces was quantified from the information provided by the spatial distribution functions of the 3D-RISM-KH theory, whereas the adsorption isotherms were not obtained from the spatial distribution functions provided. The 3D-RISM-KH molecular theory of solvation, on the other hand, is a fully fledged statistical-mechanical approach that provides complete information on the adsorption structure and thermodynamics. Therefore, even

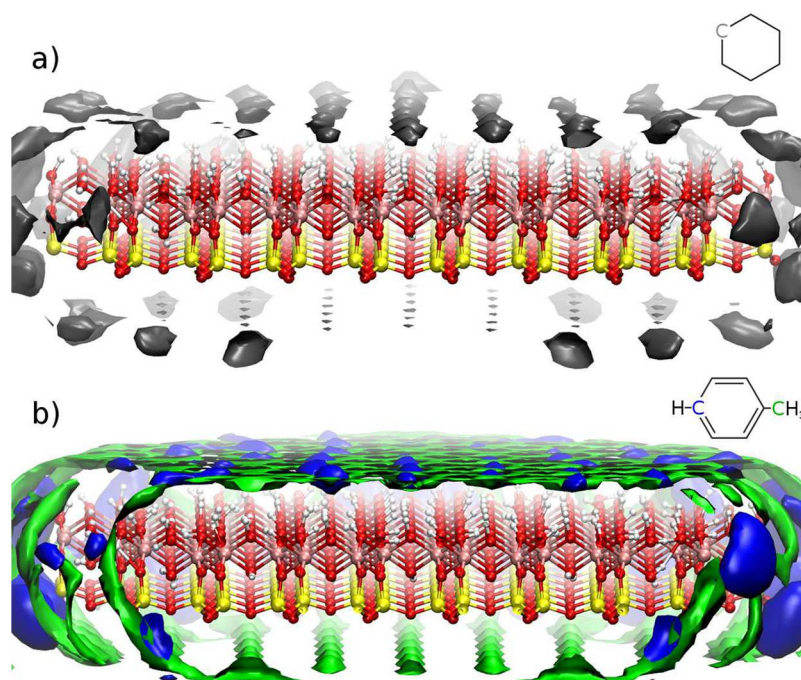


Figure 4. Solvation structure of kaolinite nanoplate in cyclohexane (a) and toluene solvents (b) predicted by the 3D-RISM-KH molecular theory of solvation. The isosurfaces are presented for the spatial distribution functions of one of the carbon sites of cyclohexane (gray) at isovalue of 1.65 in (a) and for the distribution functions of the terminal (green) and ring (blue) carbon sites of toluene at isovalue of 2.5 in (b).

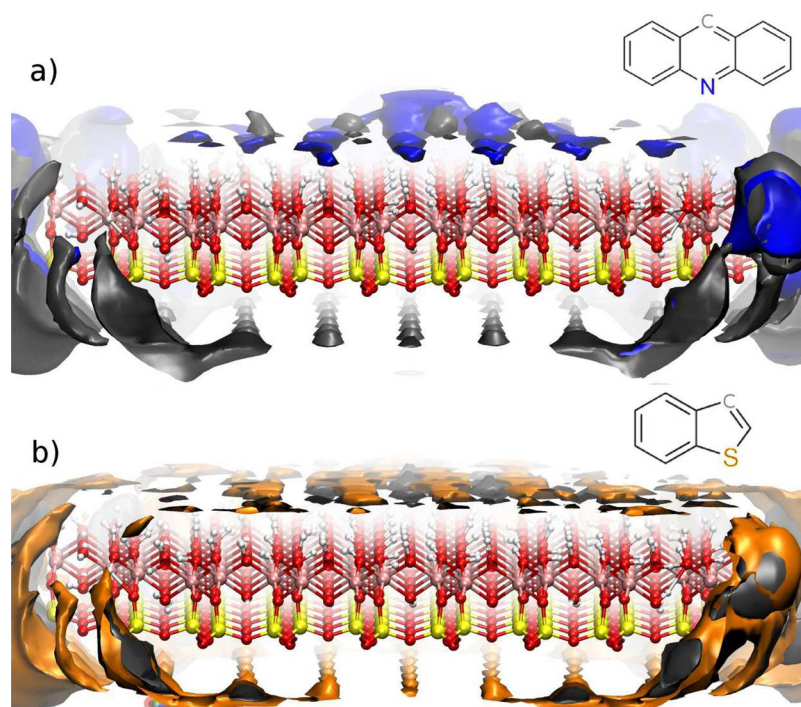


Figure 5. Adsorption structure of acridine (a) and benzothiophene (b) on kaolinite nanoplate in cyclohexane solvent predicted by the 3D-RISM-KH molecular theory of solvation. The isosurfaces are respectively presented for the spatial distribution functions of N site (blue) and the opposite carbon site (gray) of acridine (a) at isovalues of 4 and 3.1, and for the distribution functions of S site (orange) and the opposite carbon site (gray) of benzothiophene (b) at isovalues of 3.5 and 3.5.

though the 3D-RISM-KH theory is not formulated in the grand canonical ensemble and is not widely used in the adsorption community, it is still possible to obtain the isotherms of molecular adsorption in complex solvents using a simple scheme presented in Figure 2. We propose to estimate the adsorption amount in cylindrical areas near the center of

kaolinite surfaces and to obtain the excess number of adsorbed molecules per surface area depending on the loading according to eq 6 (see also Figure 2). From eq 6, it is evident that nonzero contribution occurs only in the solvation shell of the kaolinite platelet, where the spatial distribution function differs from unity. It is also important to note that while the 3D

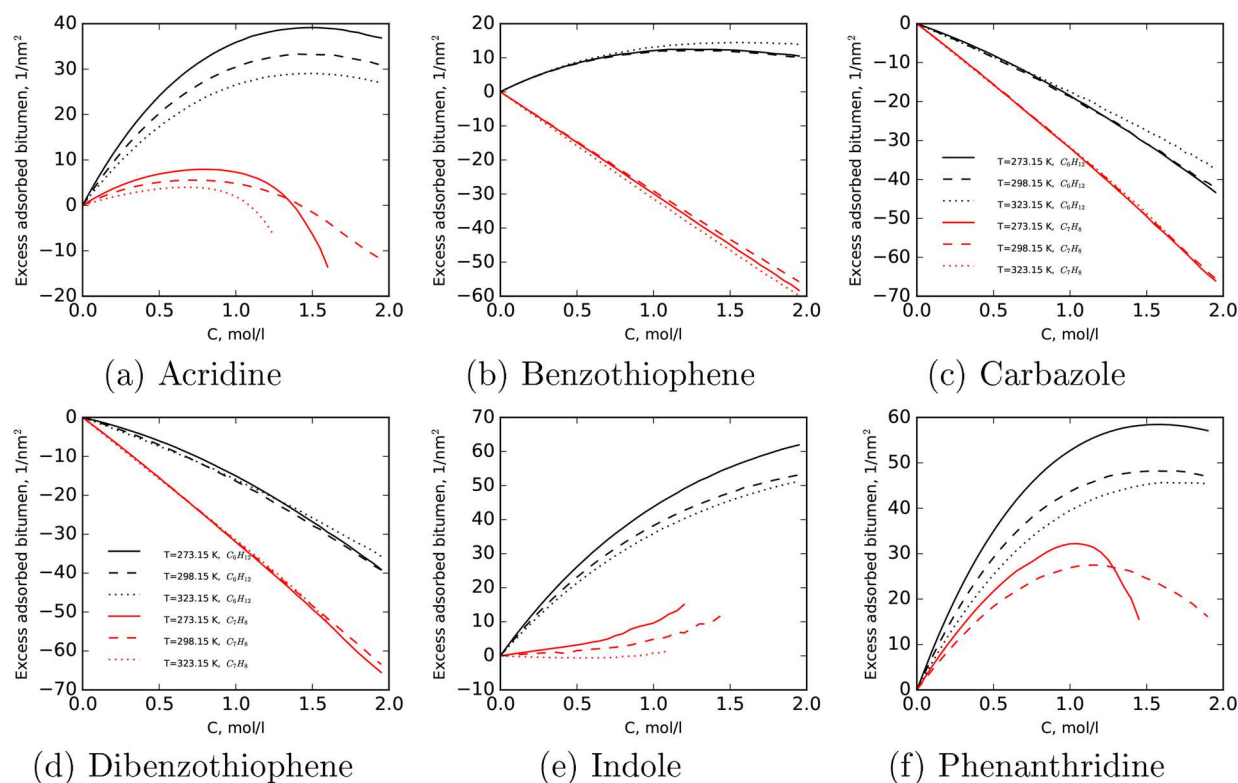


Figure 6. Excess number of adsorbed HAC molecules per unit of surface area of silicon oxide surface at three different temperatures, 273.15 (solid line), 293.15 (dashed line), and 323.15 K (dotted line), in cyclohexane (black) and toluene (red) solvents.

density distributions of the individual sites around kaolinite nanoplate predicted by the 3D-RISM-KH theory are mutually correlated through the 3D-RISM equation (eq 1), the correlation assumes RISM-like spherical symmetry of the sites with respect to each other; i.e., only the distance between every pair of sites is preserved by the theory. This kind of approximation, however, is also common in other density functional theories of polyatomic molecules.⁷⁰ The performance and accuracy of the RISM and 3D-RISM theories is well studied and documented.^{41,71}

More information on the molecule–surface interactions of acridine and benzothiophene with kaolinite could be obtained in Figure 5, where the isosurfaces of the density distribution functions of N, S, and C sites of these HACs are presented. From the examination of the isosurfaces, it is clear that the bitumen fragments exhibit strong adsorption at the exposed active sites of the edges of the kaolinite nanoparticle. However, taking into account the effect of the edges on the adsorption is out of the scope of the present study. Chemical properties of the exposed active sites at the edges of kaolinite nanoparticle are different than the properties of their bulk counterparts. Proper description of the exposed active sites requires additional modeling effort, which will be addressed in forthcoming contributions. In the current work, we tried to minimize the contribution of the edges into the adsorption isotherms by calculating the integral of eq 6 only in the central region of the platelet. Analysis of the isosurfaces near the flat kaolinite surfaces reveals that both the N site of acridine and the S site of benzothiophene show significant accumulation near the aluminum hydroxide surface. Additionally, the S atom of benzothiophene shows also some density enhancements near the centers of the Si–O hexagonal rings of the silicon oxide surface. Strong attraction of the pyridinic N sites to the

aluminum hydroxide surface is explained by the hydrogen bonding with the laterally oriented hydroxyl groups of the surface. On the other hand, the density enhancements of the S atom of benzothiophene are mostly observed near the axially oriented hydroxyl groups or in places where hydroxyl oxygen sites are exposed. By examining the relative positions of density enhancements of N, S, and C sites of the adsorbed molecules, one could also obtain insights on the orientation of the adsorbed molecules. Thus, the slightly more distant location of density enhancements of C sites compared to N sites of acridine suggests a possible nonparallel orientation of the latter, which can be explained by hydrogen bonding of the pyridinic N atom of acridine with the H atom of axially oriented surface hydroxyl groups. Similar analysis of the locations of S and C sites of benzothiophene suggests domination of parallel orientations of the molecules to the aluminum hydroxide surface of kaolinite. These orientations are favored due to cumulative action of electrostatic, dispersive, and solvation interactions. For more detailed information on the molecule surface recognition interactions of HACs and kaolinite in toluene, interested readers are directed to the recent studies by Huang et al. and Fafard et al.^{24,25} In the discussion below we will focus mainly on the analysis of effective interactions between kaolinite nanoparticles, and estimation (comparison) of adsorption isotherms of HACs in cyclohexane and toluene solvents.

By integrating the spatial distribution functions using the scheme proposed in Figure 2, we have calculated the excess adsorption isotherms of bitumen fragments on kaolinite at different solvent conditions and several temperatures. The excess adsorption isotherms for acridine, benzothiophene, carbazole, dibenzothiophene, indole, and phenanthridine HAC bitumen fragments are presented for the silicon oxide

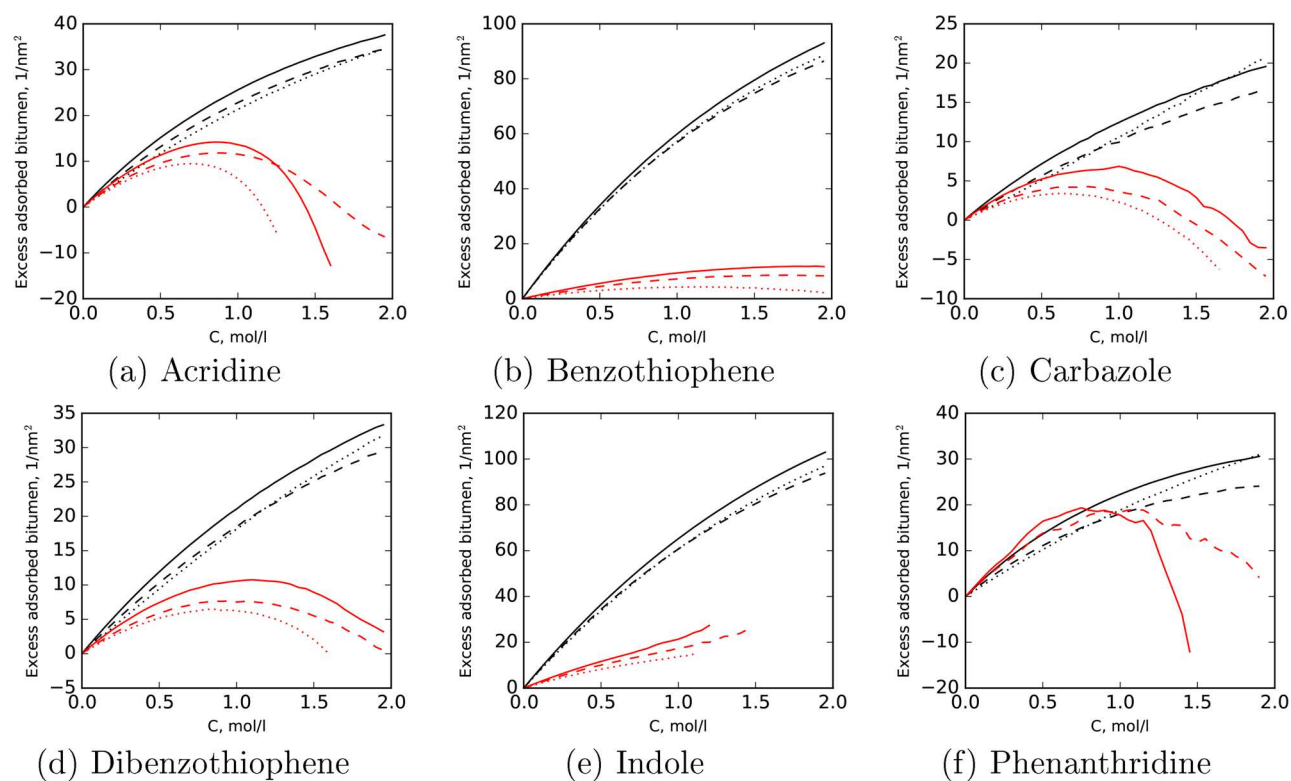


Figure 7. Excess number of adsorbed HAC molecules per unit of surface area of aluminum hydroxide surface at three different temperatures, 273.15 (solid line), 293.15 (dashed line), and 323.15 K (dotted line), in cyclohexane (black) and toluene (red) solvents.

surface of kaolinite in Figure 6, parts a, b, c, d, e, and f, respectively, and for the aluminum hydroxide surface of kaolinite in Figure 7, parts a, b, c, d, e, and f, respectively. Similarly to the picture of adsorption of the bitumen fragments in toluene,²⁴ the tetrahedral siloxane surface appears to be less preferable for the adsorption of the bitumen fragments than the octahedral surface. This prediction could be clearly observed in the lateral distribution function profiles of the HACs presented in Figure 3 for cyclohexane and toluene solvents. The adsorption structure of the HACs in cyclohexane and toluene are quite similar, as they both show predominant adsorption of HACs on the octahedral aluminum hydroxide surface. The main difference between the profiles is in the magnitude of the surface peaks of the HAC distribution functions, which are higher for cyclohexane than for toluene solvent. This fact suggests that adsorption of the studied HACs is stronger in cyclohexane than in toluene. Indeed, the solvent distribution profiles show stronger adsorption of toluene than cyclohexane at the aluminum hydroxide surface of kaolinite. Toluene seems to compete with HACs for the adsorption surface on the aluminum hydroxide face of kaolinite, and, therefore, might weaken the adsorption of the fragments. This observation, however, does not fully explain the stronger adsorption of HACs on the silicon oxide surface in cyclohexane than in toluene, as in this case both solvents show comparable surface solvation. Therefore, the difference in the predicted adsorption strengths must be due to a better solvation of the studied HACs by toluene. Indeed, it is well-known that acridine is more soluble in aromatic benzene than in aliphatic cyclohexane.⁷²

The distribution function profiles suggest that the tetrahedral silicon oxide surface is much less preferable for the adsorption of HACs and solvents when compared to the aluminum hydroxide surface. However, the excess adsorption of bitumen

HAC fragments on the siloxane surface is not negative (a negative value corresponds to the depletion of molecules from the surface), but is, in fact, positive in both solvents for acridine, indole, and phenanthridine. In the latter case, the number of excessively adsorbed molecules is predicted to be higher on the siloxane surface, even though the interaction with the aluminum hydroxide surface is expected to be stronger due to the hydrogen bonding interactions of surface hydroxyl groups with pyridinic N sites. The main contribution into the excess adsorption on the siloxane surface in cyclohexane comes from the second adsorption layers of HACs, which are generally higher and wider than the first layers. Therefore, the adsorption of HACs on the siloxane tetrahedral surface predicted by the 3D-RISM-KH molecular theory of solvation can be described as a two-layer adsorption with the weakly adsorbed first layer and significantly wider second layer. The latter is responsible for the main contribution into the excess isotherms. It is also important to note that the second adsorption layer of HACs is not so well pronounced in toluene solvent.

A general picture of the adsorption on the aluminum hydroxide surface is more conventional. It is dominated by strong hydrogen bonding interactions of surface hydroxyl groups with the active sites of the HACs. A more detailed analysis of the adsorption configurations of the heterocycles on kaolinite in toluene solvent and the role of hydrogen bonding in the adsorption of the HACs on the aluminum hydroxide surface was conducted by Huang et al.²⁵ The main difference of the adsorption picture in cyclohexane consists in a stronger effective interaction of the studied HACs with the surface due to weaker solvation properties of this aliphatic solvent.

Both kaolinite surfaces exhibit decrease of the amount of adsorbed bitumen fragments with temperature increase, as the latter makes the molecule–surface interactions less significant

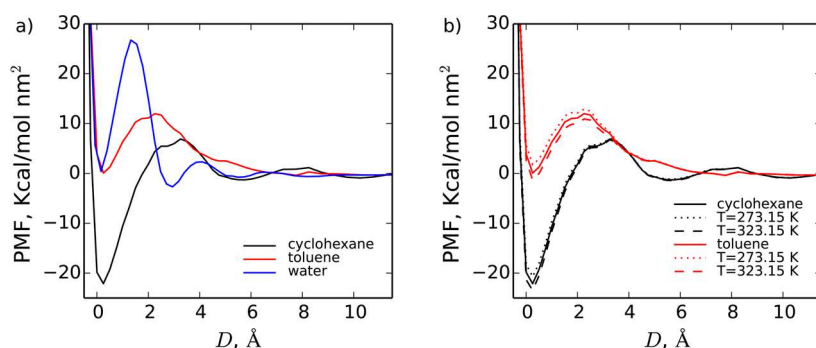


Figure 8. Potential of mean force between nanoparticles in pure cyclohexane, water, and toluene solvents at 298.15 K (a) and a comparison of PMFs at 273.15, 298.15, and 323.15 K (b).

compared to the entropic free energy. Therefore, the main conclusion is that the elevated temperatures should facilitate the desorption of HACs from kaolinite surfaces. This conclusion should also generalize to larger bitumen macromolecules. However, the temperatures above 25 °C might be not viable for the bitumen extraction process, as excellent extraction performance (above 90%) was already achieved at room temperatures⁸ for cyclohexane and several other organic solvents. Moreover, the main advantage of the nonaqueous extraction in terms of decreased energy use and CO₂ emissions will be lost when operated at increased temperatures.

Potential of Mean Force between Nanoparticles. In order to assess the effects of solvents and temperature on the flocculation behavior of the kaolinite fines in organic solutions, we have calculated PMFs per surface area between different surfaces of kaolinite nanoparticles in several solutions of HACs in organic solvents at several temperatures. The PMFs of kaolinite nanoparticles in pure water, cyclohexane, and toluene are compared in Figure 8a. The presented PMFs correspond to the free energy of delamination/exfoliation of the two-layered kaolinite sheet into two single sheets. They demonstrate a striking difference between the effective interactions in aqueous and organic solvents. The main observation is that the first defoliation/disaggregation barrier is much less significant for organic solvents than for water. This fact can be explained by a higher surface hydration energy, when compared to the solvation energies of toluene and cyclohexane solvents. Both organic solvents also produce wider oscillations of the PMFs, which is due to the larger size of cyclohexane and toluene molecules when compared to the water molecule. The first minimum of the PMF, which corresponds to the direct contact of the interacting surfaces, is much deeper in cyclohexane solvent than in toluene and water. This suggests that the state of direct contact between the nanoparticles in cyclohexane is clearly a stable equilibrium state, as the corresponding energy of the minimum is negative, and also as the solvation of kaolinite surfaces is weaker in cyclohexane than in the other two solvents. Indeed, the larger is the adsorption energy of molecules, the more energy is required to clean the surfaces when bringing them to the contact. Thus, the strong solvation contributes positively to the PMF, as the stronger solvent–surface interactions generally lead to higher PMFs between the particles at short ranges. Significantly stronger solvation of the aluminum hydroxide surface by toluene (when compared to cyclohexane) can be deduced from the laterally averaged distribution functions in Figure 3. Stronger solvation of the surfaces in toluene provides an explanation of a more repulsive character of the PMFs observed in this organic solvent.

The energy barrier separating the first and the second minima represents the activation energy relevant to the kinetics of exfoliation. The first barrier seems to be highest for water, followed by toluene and cyclohexane. However, because the latter case has the deepest first minimum, the corresponding activation energy required to detach (exfoliate) the nanoparticles from the state of direct contact in cyclohexane is comparable to the one observed in aqueous solutions. The smallest activation energy of defoliation is predicted for toluene solvent, and is only about 11 kcal/mol·nm². The position of the barrier relative to the first minimum seems to be determined by the effective size of the solvent molecules. The most distant barrier is observed for cyclohexane, followed by toluene and water. Interestingly, even though toluene and cyclohexane are comparable in size (toluene is slightly longer and more planar, while cyclohexane is thicker), the barrier for the latter appears to be more separated from the first minimum. This fact suggests that the solvent molecules in the first layer are oriented parallel to the surface. The height of the barrier, on the other hand, is largely determined by the strength of the solvent–surface interactions. Thus, the better packing and the higher density of toluene molecules near the surface, the higher PMF barrier in this solvent.

Both cyclohexane and water PMFs possess well-defined second minima, which correspond to the solvent separated contact state, i.e., the state when the surfaces are separated by a single layer of solvent. Surprisingly, the second minimum is not predicted for the nanoparticles in toluene. Instead, the PMF gradually decays to zero without much oscillation.

The effect of temperature on the PMF between nanoparticles is examined in Figure 8b. The PMFs for both cyclohexane and toluene increase slightly as temperature is dropped from $T = 323.15$ K to $T = 298.15$ K, and then to $T = 273.15$ K. The strength of the effective interactions between the surfaces and the solvents weakens as temperature increases, which leads to the decrease of the solvation free energy of the surfaces. This in turn leads to the decrease of PMF, as the latter largely depends on the work required to desolvate the surfaces when bringing them together. Therefore, while the elevated temperatures are most probably not viable for enhanced desorption of bitumen, they might be useful for coagulation of the fines. In the latter case, an addition of coagulant/adjuvant might be required, as the sole effect of temperature on the PMFs between the clay nanoparticles does not seem to be significant for the studied temperature differences. Moreover, by operating at elevated temperatures the main advantages of nonaqueous extraction in terms of decreasing energy use and CO₂ emissions will be lost.

The impact of the adsorption of bitumen HAC fragments on the PMF between the nanoparticles is examined in Figure 9.

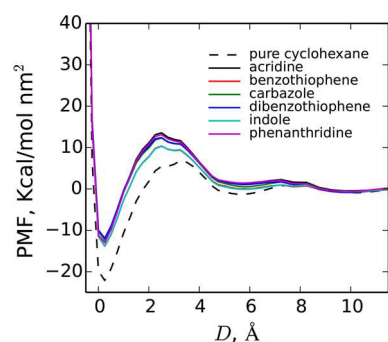


Figure 9. Potential of mean force between nanoparticles in pure cyclohexane and in cyclohexane with HAC bitumen fragments (at concentration of 1.5 mol/L).

Adsorption of the studied HACs on the interacting surfaces leads to an increase of the PMF at short separations. In order to squeeze the surfaces together, one has to remove the adsorbed HACs. This fact leads to the increase of the PMF, as the energy required to remove pure cyclohexane is smaller than the energy required to remove HACs due to the stronger adsorption of the latter. Taking into account that during coagulation kaolinite forms book-like aggregates in both aqueous⁷³ and non-aqueous⁷⁴ solutions, one could speculate that adsorption of bitumen tends to stabilize the suspension. The latter follows from the increase of the first PMF barrier, which should in turn decrease the tendency of formation of face–face associations of kaolinite nanoparticles. This conclusion, however, should be taken with a grain of salt, as the coagulation pathway in the presence of bitumen might be different from the one in pure solvents, and formation of the book-like aggregates might not be favored.

CONCLUSIONS

Molecular models of kaolinite clay nanoplatelets in organic solutions of cyclohexane and toluene solvents together with bitumen fragments represented by several heterocyclic aromatic compounds (HACs) were developed. Using the 3D-RISM-KH molecular theory of solvation, preferential adsorption of the fragments on the clay surfaces and the solvent-mediated effective interactions between kaolinite nanoparticles were investigated. The main trend of adsorption consisted in preferential adsorption of the studied bitumen fragments on the aluminum hydroxide face of kaolinite, and weaker more selective adsorption on the siloxane face of the nanoparticle.

In order to quantitatively compare the amount of adsorbed molecules on the two surfaces of kaolinite, excess adsorption isotherms of bitumen HAC fragments in cyclohexane and toluene solvents were calculated at several temperatures. The theory predicts generally stronger adsorption of the fragments on the aluminum hydroxide surface of kaolinite in both organic solvents. The adsorption, however, was predicted to be stronger in cyclohexane than in toluene solvent, which might be explained by a better surface and molecule solvation properties of toluene. Temperature increase generally leads to a weaker adsorption of the bitumen HAC fragments in the studied organic solvents.

All-atom molecular description of the solution species and kaolinite nanoparticles using the 3D-RISM-KH molecular

theory of solvation takes into account the effects of chemical specificities and structural properties of solution species on the PMF. Application of the 3D-RISM-KH theory allowed identification of solvation-related effects in the effective interactions of clay nanoparticles in solution. As a result, the calculated PMFs between kaolinite nanoparticles exhibited an oscillating behavior at short ranges with characteristic solvation and aggregation energy barriers. The first barrier height relative to the second minimum characterizes the free energy required to desolvate the surfaces when bringing the nanoparticles into contact with each other. The height of the barrier relative to the first minimum describes the energy required to move the nanoparticles against the solution environment and to create a desolvation cavity between them. The second minimum of the PMF in cyclohexane, which corresponds to a solvent-separated contact state of interacting nanoparticles, is much shallower than the first minima. The second minimum, however, is missing from the predicted PMFs in toluene. Moreover, the first minimum of the PMF in this aromatic solvent is much shallower than in cyclohexane solvent. These observations clearly indicate the importance of the solvent effects on the aggregation properties of mineral suspensions.

Similarly to the picture of bitumen HAC fragment adsorption, temperature increase generally leads to the decrease of the PMF in pure organic solvents. This decrease, however, is quite modest and seems to be mostly due to a temperature-induced weakening of the surface solvation energies.

AUTHOR INFORMATION

Corresponding Author

*E-mail: andriy.kovalenko@ualberta.ca.

ORCID

Andriy Kovalenko: 0000-0001-5033-4314

Notes

The authors declare no competing financial interest.

ACKNOWLEDGMENTS

This work was supported by the Institute for Oil Sand Innovation (IOSI) at the University of Alberta and by the National Institute for Nanotechnology, National Research Council of Canada. The authors thank Prof. Christian Detellier, Department of Chemistry, University of Ottawa, for fruitful discussions. The high performance computing resources were provided by the WestGrid (www.westgrid.ca) and Compute Canada/Calcul Canada (www.computecanada.ca) National Advanced Computing Platform.

REFERENCES

- (1) Attanasi, E. D.; Meyer, R. F. Natural bitumen and extra-heavy oil. *Survey of Energy Resources*, 22nd ed.; Trinnaman, J., Clarke, A., Eds.; World Energy Council: London, 2010; pp 123–140.
- (2) Alboudwarej, H.; Felix, J.; Taylor, S.; Badry, R.; Bremner, C.; Brough, B.; Skeates, C.; Baker, A.; Palmer, D.; Pattison, K. Highlighting heavy oil. *Oilfield Rev.* **2006**, *18*, 34–53.
- (3) Bitumen and heavy crudes: the energy security problem solved? *Oil Energy Trends* **2006**, *31*, 3–6. DOI: 10.1111/j.1744-7992.2006.310603.x.
- (4) Newell, E. P. Canada's oilsands industry comes of age. *Oil Gas J.* **1999**, 97.
- (5) Natural Resources Canada. Canada has the third-largest proven oil reserve in the world, most of which is in the oil sands. 2017. <http://www.nrcan.gc.ca/energy/oil-sands/18085> (accessed Aug 25, 2017).
- (6) Clark, K. A. *Can. Pet.* **1966**, *7*, 18–25.

- (7) Masliyeh, J.; Czarniecki, J.; Xu, Z. *Handbook on Theory and Practice of Bitumen Recovery from Athabasca Oil Sands - Volume 1: Theoretical Basis*; Kingsley Publishing Services: 2011.
- (8) Nikakhtari, H.; Vagi, L.; Choi, P.; Liu, Q.; Gray, M. R. Solvent screening for non-aqueous extraction of Alberta oil sands. *Can. J. Chem. Eng.* **2013**, *91*, 1153–1160.
- (9) Pulati, N.; Lupinsky, A.; Miller, B.; Painter, P. Extraction of bitumen from oil sands using deep eutectic ionic liquid analogues. *Energy Fuels* **2015**, *29*, 4927–4935.
- (10) Pal, K.; Nogueira Branco, L. d. P.; Heintz, A.; Choi, P.; Liu, Q.; Seidl, P. R.; Gray, M. R. Performance of Solvent Mixtures for Non-aqueous Extraction of Alberta Oil Sands. *Energy Fuels* **2015**, *29*, 2261–2267.
- (11) Sui, H.; Zhang, J.; Yuan, Y.; He, L.; Bai, Y.; Li, X. Role of binary solvent and ionic liquid in bitumen recovery from oil sands. *Can. J. Chem. Eng.* **2016**, *94*, 1191–1196.
- (12) Yang, Z.; Nikakhtari, H.; Wolf, S.; Hu, D.; Gray, M. R.; Chou, K. C. Binary Solvents with Ethanol for Effective Bitumen Displacement at Solvent/Mineral Interfaces. *Energy Fuels* **2015**, *29*, 4222–4226.
- (13) Panda, S. Role of Residual Bitumen on the Solvent Removal from Alberta Oil Sands. Ph.D. Thesis, University of Alberta, 2015.
- (14) Boulet, P.; Greenwell, H.; Stackhouse, S.; Coveney, P. Recent advances in understanding the structure and reactivity of clays using electronic structure calculations. *J. Mol. Struct.: THEOCHEM* **2006**, *762*, 33–48.
- (15) Stoyanov, S. R.; Gusarov, S.; Kuznicki, S. M.; Kovalenko, A. Theoretical modeling of zeolite nanoparticle surface acidity for heavy oil upgrading. *J. Phys. Chem. C* **2008**, *112*, 6794–6810.
- (16) Johnson, E. R.; Otero-de-la Roza, A. Adsorption of organic molecules on kaolinite from the exchange-hole dipole moment dispersion model. *J. Chem. Theory Comput.* **2012**, *8*, 5124–5131.
- (17) Geatches, D. L.; Jacquet, A.; Clark, S. J.; Greenwell, H. C. Monomer adsorption on kaolinite: Modeling the essential ingredients. *J. Phys. Chem. C* **2012**, *116*, 22365–22374.
- (18) Lee, S. G.; Choi, J. I.; Koh, W.; Jang, S. S. Adsorption of β -D-glucose and cellobiose on kaolinite surfaces: Density functional theory (DFT) approach. *Appl. Clay Sci.* **2013**, *71*, 73–81.
- (19) Lage, M. R.; Stoyanov, S. R.; Carneiro, J. W. d. M.; Dabros, T.; Kovalenko, A. Adsorption of Bitumen Model Compounds on Kaolinite in Liquid and Supercritical Carbon Dioxide Solvents: A Study by Periodic Density Functional Theory and Molecular Theory of Solvation. *Energy Fuels* **2015**, *29*, 2853–2863.
- (20) Underwood, T.; Erastova, V.; Greenwell, H. C. Wetting Effects and Molecular Adsorption at Hydrated Kaolinite Clay Mineral Surfaces. *J. Phys. Chem. C* **2016**, *120*, 11433–11449.
- (21) Underwood, T.; Erastova, V.; Cubillas, P.; Greenwell, H. C. Molecular dynamic simulations of montmorillonite-organic interactions under varying salinity: an insight into enhanced oil recovery. *J. Phys. Chem. C* **2015**, *119*, 7282–7294.
- (22) Greathouse, J. A.; Pike, D. Q.; Greenwell, H. C.; Johnston, C. T.; Wilcox, J.; Cygan, R. T.; Geatches, D. I. Methylene Blue Adsorption on the Basal Surfaces of Kaolinite: Structure and Thermodynamics from Quantum and Classical Molecular Simulation. *Clays Clay Miner.* **2015**, *63*, 185–198.
- (23) Hlushak, S.; Stoyanov, S. R.; Kovalenko, A. A 3D-RISM-KH Molecular Theory of Solvation Study of the Effective Stacking Interactions of Kaolinite Nanoparticles in Aqueous Electrolyte Solution Containing Additives. *J. Phys. Chem. C* **2016**, *120*, 21344–21357.
- (24) Fafard, J.; Lyubimova, O.; Stoyanov, S. R.; Dedzo, G. K.; Gusarov, S.; Kovalenko, A.; Detellier, C. Adsorption of indole on kaolinite in nonaqueous media: Organoclay preparation and characterization, and 3D-RISM-KH molecular theory of solvation investigation. *J. Phys. Chem. C* **2013**, *117*, 18556–18566.
- (25) Huang, W.; Dedzo, G. K.; Stoyanov, S. R.; Lyubimova, O.; Gusarov, S.; Singh, S.; Lao, H.; Kovalenko, A.; Detellier, C. Molecule-Surface Recognition between Heterocyclic Aromatic Compounds and Kaolinite in Toluene Investigated by Molecular Theory of Solvation and Thermodynamic and Kinetic Experiments. *J. Phys. Chem. C* **2014**, *118*, 23821–23834.
- (26) Ruzicka, B.; Zaccarelli, E.; Zulian, L.; Angelini, R.; Sztucki, M.; Moussaïd, A.; Narayanan, T.; Sciortino, F. Observation of empty liquids and equilibrium gels in a colloidal clay. *Nat. Mater.* **2011**, *10*, 56–60.
- (27) Tanaka, H.; Meunier, J.; Bonn, D. Nonergodic states of charged colloidal suspensions: repulsive and attractive glasses and gels. *Phys. Rev. E: Stat. Phys., Plasmas, Fluids, Relat. Interdiscip. Top.* **2004**, *69*, 031404.
- (28) Fossum, J. O. Physical phenomena in clays. *Phys. A (Amsterdam, Neth.)* **1999**, *270*, 270–277.
- (29) Mouchid, A.; Lecolier, E.; Van Damme, H.; Levitz, P. On viscoelastic, birefringent, and swelling properties of Laponite clay suspensions: revisited phase diagram. *Langmuir* **1998**, *14*, 4718–4723.
- (30) Dijkstra, M.; Hansen, J.; Madden, P. Gelation of a clay colloid suspension. *Phys. Rev. Lett.* **1995**, *75*, 2236.
- (31) Dijkstra, M.; Hansen, J.-P.; Madden, P. A. Statistical model for the structure and gelation of smectite clay suspensions. *Phys. Rev. E: Stat. Phys., Plasmas, Fluids, Relat. Interdiscip. Top.* **1997**, *55*, 3044.
- (32) Hofmann, U.; Fahn, R.; Weiss, A. Thixotropie bei Kaolinit und innerkristalline Quellung bei Montmorillonit. *Colloid Polym. Sci.* **1957**, *151*, 97–115.
- (33) Van Olphen, H. Rheological phenomena of clay sols in connection with the charge distribution on the micelles. *Discuss. Faraday Soc.* **1951**, *11*, 82–84.
- (34) Jonsson, B.; Labbez, C.; Cabane, B. Interaction of nanometric clay platelets. *Langmuir* **2008**, *24*, 11406–11413.
- (35) Delhomme, M.; Jönsson, B.; Labbez, C. Monte Carlo simulations of a clay inspired model suspension: the role of rim charge. *Soft Matter* **2012**, *8*, 9691–9704.
- (36) Delhomme, M.; Jönsson, B.; Labbez, C. Gel, glass and nematic states of plate-like particle suspensions: charge anisotropy and size effects. *RSC Adv.* **2014**, *4*, 34793–34800.
- (37) Shalkevich, A.; Stradner, A.; Bhat, S. K.; Muller, F.; Schurtenberger, P. Cluster, glass, and gel formation and viscoelastic phase separation in aqueous clay suspensions. *Langmuir* **2007**, *23*, 3570–3580.
- (38) Kovalenko, A.; Hirata, F. Potentials of mean force of simple ions in ambient aqueous solution. I. Three-dimensional reference interaction site model approach. *J. Chem. Phys.* **2000**, *112*, 10391–10402.
- (39) Kovalenko, A.; Hirata, F. Potentials of mean force of simple ions in ambient aqueous solution. II. Solvation structure from the three-dimensional reference interaction site model approach, and comparison with simulations. *J. Chem. Phys.* **2000**, *112*, 10403–10417.
- (40) Kovalenko, A. Multiscale modeling of solvation in chemical and biological nanosystems and in nanoporous materials. *Pure Appl. Chem.* **2013**, *85*, 159–199.
- (41) Kovalenko, A. Multiscale modeling of solvation. In *Springer Handbook of Electrochemical Energy*; Breitkopf, K., Swider-Lyons, K., Eds.; Springer: Berlin, 2017; pp 95–139.
- (42) Yoshida, K.; Yamaguchi, T.; Kovalenko, A.; Hirata, F. Structure of tert-butyl alcohol-water mixtures studied by the RISM theory. *J. Phys. Chem. B* **2002**, *106*, 5042–5049.
- (43) Kovalenko, A.; Hirata, F. Towards a molecular theory for the van der Waals-Maxwell description of fluid phase transitions. *J. Theor. Comput. Chem.* **2002**, *01*, 381–406.
- (44) Kovalenko, A. In *Molecular Theory of Solvation*; Hirata, F., Ed.; Springer: 2003; pp 169–275.
- (45) da Costa, L. M.; Hayaki, S.; Stoyanov, S. R.; Gusarov, S.; Tan, X.; Gray, M. R.; Stryker, J. M.; Tykewinski, R.; Carneiro, J. d. M.; Sato, H.; et al. 3D-RISM-KH molecular theory of solvation and density functional theory investigation of the role of water in the aggregation of model asphaltene. *Phys. Chem. Chem. Phys.* **2012**, *14*, 3922–3934.
- (46) Johnson, R. S.; Yamazaki, T.; Kovalenko, A.; Fenniri, H. Molecular basis for water-promoted supramolecular chirality inversion in helical rosette nanotubes. *J. Am. Chem. Soc.* **2007**, *129*, 5735–5743.

- (47) Kovalenko, A.; Kobryn, A. E.; Gusarov, S.; Lyubimova, O.; Liu, X.; Blinov, N.; Yoshida, M. Molecular theory of solvation for supramolecules and soft matter structures: application to ligand binding, ion channels, and oligomeric polyelectrolyte gelators. *Soft Matter* **2012**, *8*, 1508–1520.
- (48) Yamazaki, T.; Kovalenko, A. Spatial decomposition analysis of the thermodynamics of cyclodextrin complexation. *J. Chem. Theory Comput.* **2009**, *5*, 1723–1730.
- (49) Silveira, R. L.; Stoyanov, S. R.; Gusarov, S.; Skaf, M. S.; Kovalenko, A. Plant biomass recalcitrance: effect of hemicellulose composition on nanoscale forces that control cell wall strength. *J. Am. Chem. Soc.* **2013**, *135*, 19048–19051.
- (50) Chandler, D.; McCoy, J. D.; Singer, S. J. Density functional theory of nonuniform polyatomic systems. I. General formulation. *J. Chem. Phys.* **1986**, *85*, 5971–5976.
- (51) Chandler, D.; McCoy, J. D.; Singer, S. J. Density functional theory of nonuniform polyatomic systems. II. Rational closures for integral equations. *J. Chem. Phys.* **1986**, *85*, 5977–5982.
- (52) Beglov, D.; Roux, B. An integral equation to describe the solvation of polar molecules in liquid water. *J. Phys. Chem. B* **1997**, *101*, 7821–7826.
- (53) Kovalenko, A.; Hirata, F. Three-dimensional density profiles of water in contact with a solute of arbitrary shape: a RISM approach. *Chem. Phys. Lett.* **1998**, *290*, 237–244.
- (54) Kovalenko, A.; Hirata, F. Self-consistent description of a metal–water interface by the Kohn–Sham density functional theory and the three-dimensional reference interaction site model. *J. Chem. Phys.* **1999**, *110*, 10095–10112.
- (55) Kovalenko, A.; Hirata, F. Potentials of mean force of simple ions in ambient aqueous solution. I. Three-dimensional reference interaction site model approach. *J. Chem. Phys.* **2000**, *112*, 10391–10402.
- (56) Kovalenko, A.; Hirata, F. Potentials of mean force of simple ions in ambient aqueous solution. II. Solvation structure from the three-dimensional reference interaction site model approach, and comparison with simulations. *J. Chem. Phys.* **2000**, *112*, 10403–10417.
- (57) Kovalenko, A. In *Molecular Theory of Solvation*; Hirata, F., Ed.; Springer: 2003; pp 169–275.
- (58) Gusarov, S.; Pujari, B. S.; Kovalenko, A. Efficient treatment of solvation shells in 3D molecular theory of solvation. *J. Comput. Chem.* **2012**, *33*, 1478–1494.
- (59) Kovalenko, A. Multiscale modeling of solvation in chemical and biological nanosystems and in nanoporous materials. *Pure Appl. Chem.* **2013**, *85*, 159–199.
- (60) Hansen, J.-P.; McDonald, I. R. *Theory of Simple Liquids*, 3rd ed.; Academic Press: 2006.
- (61) Lang, A.; Kahl, G.; Likos, C. N.; Löwen, H.; Watzlawek, M. Structure and thermodynamics of square-well and square-shoulder fluids. *J. Phys.: Condens. Matter* **1999**, *11*, 10143.
- (62) Hlushak, S. P.; Hlushak, P.; Trokhymchuk, A. An improved first-order mean spherical approximation theory for the square-shoulder fluid. *J. Chem. Phys.* **2013**, *138*, 164107.
- (63) Hlushak, S.; Trokhymchuk, A. Simplified exponential approximation for thermodynamics of a hard-core repulsive Yukawa fluid. *Condens. Matter Phys.* **2012**, *15*, 23003.
- (64) Hlushak, S. Exponential approximation for one-component Yukawa plasma. *J. Chem. Phys.* **2014**, *141*, 204108.
- (65) Perkyns, J. S.; Lynch, G. C.; Howard, J. J.; Pettitt, B. M. Protein solvation from theory and simulation: Exact treatment of Coulomb interactions in three-dimensional theories. *J. Chem. Phys.* **2010**, *132*, 064106.
- (66) Stewart, J. J. Optimization of parameters for semiempirical methods VI: more modifications to the NDDO approximations and re-optimization of parameters. *J. Mol. Model.* **2013**, *19*, 1–32.
- (67) Plimpton, S. Fast parallel algorithms for short-range molecular dynamics. *J. Comput. Phys.* **1995**, *117*, 1–19.
- (68) Cygan, R. T.; Liang, J.-J.; Kalinichev, A. G. Molecular models of hydroxide, oxyhydroxide, and clay phases and the development of a general force field. *J. Phys. Chem. B* **2004**, *108*, 1255–1266.
- (69) Gupta, V.; Miller, J. D. Surface force measurements at the basal planes of ordered kaolinite particles. *J. Colloid Interface Sci.* **2010**, *344*, 362–371.
- (70) Yu, Y.-X.; Wu, J. Density functional theory for inhomogeneous mixtures of polymeric fluids. *J. Chem. Phys.* **2002**, *117*, 2368–2376.
- (71) Hirata, F. *Molecular Theory of Solvation*; Springer Science & Business Media: 2003; Vol. 24.
- (72) Acree, W. Polycyclic Aromatic Hydrocarbons: Binary Non-aqueous Systems. *Solubility Data Ser.* **1995**, 58–59.
- (73) Gupta, V.; Hampton, M. A.; Stokes, J. R.; Nguyen, A. V.; Miller, J. D. Particle interactions in kaolinite suspensions and corresponding aggregate structures. *J. Colloid Interface Sci.* **2011**, *359*, 95–103.
- (74) Fafard, J. Adsorption and desorption behaviour of organic molecules on kaolinite particles in non-aqueous media. Ph.D. Thesis, Université d'Ottawa/University of Ottawa, 2012.